IEEE Access
Multidisciplinary ⋮ Rapid Review ⋮ Open Access Journal

Received 15 April 2024, accepted 1 May 2024, date of publication 6 May 2024, date of current version 13 May 2024.

Digital Object Identifier 10.1109/ACCESS.2024.3397210

RESEARCH ARTICLE

Comparing Copper With Stainless Steel as a Stabilizer Layer in Resistive Superconducting Fault Current Limiters

HAMOUD ALAFNAN[1], DOAA M. YEHIA[2], ABDULLAH ALBAKER[1], AND AYOOB ALATEEQ[1]

[1]Department of Electrical Engineering, College of Engineering, University of Ha'il, Hail 55476, Saudi Arabia
[2]Department of Electrical Power and Machines Engineering, Faculty of Engineering, Tanta University, Tanta 31511, Egypt

Corresponding author: Hamoud Alafnan (h.alafnan@uoh.edu.sa)

This work was supported by the Scientific Research Deanship at the University of Ha'il, Saudi Arabia, under Project BA-23 003.

ABSTRACT The increasing penetration of renewable energy sources (RESs) into electrical networks offers several interesting opportunities and challenges. One such opportunity is the utilization of DC transmission lines, which can enhance the efficiency and reliability of power transmission. However, DC transmission lines face a challenge in dealing with fault currents due to their high magnitudes and the absence of zero crossing points, characteristics that make it difficult for DC circuit breakers (CBs) to clear faults. Resistive superconducting fault current limiters (r-SFCLs) effectively minimize high magnitude fault currents, allowing DC CBs to operate safely during fault scenarios. The self-triggering feature and fast fault current limitation ability of r-SFCLs also make them particularly suitable for protecting against high DC fault currents. Several studies demonstrated the performance of r-SFCLs with one type of stabilizer layer, most commonly using either copper (Cu) or stainless steel (SS). This paper investigates and compares the performance of an r-SFCL with the two different stabilizer layers, with one case using copper and the other using stainless steel. A thermoelectric r-SFCL model incorporating all composed layers has been developed in Simulink/MATLAB® to investigate the performance of the r-SFCLs with the two different stabilizer layers. The r-SFCLs have been evaluated using different fault scenarios applied to the DC transmission lines of a solar farm. In this model, all r-SFCL layers, excluding the stabilizer layer but including the superconducting, silver, and substrate layers, have been fixed to show the impact of the stabilizer layer materials on the r-SFCL's performance. This paper illustrates the fault current limiting capability of the r-SFCL, its effect on voltage behavior, its operating temperature, and its sensitivity to the fault location with the two different stabilizer layers. To simulate a range of fault levels and assess the limitation capability of the r-SFCLs, three distinct fault locations have been considered: one located 5 km away from the solar farm, another 15 km away, and a third 25 km away.

INDEX TERMS Resistive superconducting fault current limiter (r-SFCL), stabilizer layer, solar farm, DC transmission lines, stainless steel.

NOMENCLATURES AN ACRONYMS

A	cross-sectional area.
Ag	silver layer.
A_x	cross-sectional area of x layer.
CBs	circuit breakers.
C_p	cumulative heat capacity of the layers.
C_{px}	heat capacity of x material.
Cu	copper.
C_x	specific heat capacity of x material.

The associate editor coordinating the review of this manuscript and approving it for publication was Ali Raza.

E_c	standard electrical field.
ESSs	energy storage systems.
HTS	High-temperature superconductivity.
I	actual current.
I_c	critical current.
J_c	critical current density.
L	length.
LN_2	liquid nitrogen.
PV	photovoltaic.
Q_{sc}	net tape power.
RESs	renewable energy sources.
R_x	resistance of each layer.
SC	superconducting layer.
SMES	superconducting magnetic energy storage.
SS	stainless steel.
T	actual temperature.
T_c	critical temperature.
T_o	operating temperature.
P_{diss}	electrical losses.
$P_{cooling}$	energy absorbed through the coolant.
V_x	volume of x material.
YBCO	Yttrium Barium Copper Oxide.
d	cable diameter.
d_x	density of x material.
h	heat transfer coefficient between the tape and the LN_2 coolant.
i-SFCLs	inductive superconducting fault current limiters.
r-SFCLs	resistive superconducting fault current.
s	distance between two conductors.
α	density exponent.
μ_r	relative permeability.
μ_0	permeability of free space.
ρ_{Ag}	Silver resistivity.
ρ_{cu}	copper resistivity.
ρ_{Hast}	Hastelloy resistivity.
ρ_{ss}	Stainless steel resistivity.
ρ_x	resistivity of x layer.
ρ_{YBCO}	Yttrium barium copper oxide resistivity.

I. INTRODUCTION

A. BACKGROUND AND MOTIVATION

The high penetration of renewable energy sources (RESs) in electrical grids has led to significant changes in the design and operation of power systems. One notable change is the inherent DC output of some RESs, such as photovoltaic (PV) arrays and fuel cells. Additionally, energy storage systems (ESSs) also generate DC output. This prompted the growing use of DC microgrids and DC transmission lines. By adopting DC-based architectures, the number of power electronic converters required for the integration of RESs and ESSs can be significantly reduced or even eliminated, thereby enhancing the overall power system's efficiency [1]. However, DC systems face challenges in having high fault magnitudes as well as the absence of zero crossing points [2]. These pose a challenge to power system protection, as existing protection devices may not be able to handle the high fault currents, leading to catastrophic consequences.

Due to their self-triggering, fast operation, and effective fault current limitation ability, resistive superconducting fault current limiters (r-SFCLs) are considered an effective solution to reduce the magnitude of DC fault currents. With this reduction in the fault current magnitude, the stress on the DC CBs and other system components is minimized. There are several r-SFCLs that use different materials. Two of the most widely used superconducting tapes in the construction of r-SFCLs are SCS12050, made by SuperPower Inc. [3], and AMSC-8602, made by American Superconductor [4]. SCS12050 consists of several layers, including the superconducting layer (SC), silver layer (Ag), Hastelloy substrate layer, and two copper (Cu) stabilizer layers, as shown in Fig. 1(a). AMSC-8602 consists of several layers: superconducting (SC), silver (Ag), NiW substrate, and two stainless steel (SS) stabilizer layers.

The main motivation of this paper is to investigate and compare the existing copper stabilizer-based r-SFCL being developed by SuperPower Inc. [3] with the proposed stainless steel stabilizer-based r-SFCL in terms of fault current limiting capability, voltage behaviors, operating temperature, and sensitivity to the fault location. All other layers, including the superconducting, silver, and substrate layers, have been fixed to observe the impact of the stabilizer layer materials. The electrical representation of the r-SFCL with copper stabilizer is shown in Fig. 1 (a) and the electrical representation of the r-SFCL with stainless stabilizer is shown in Fig. 1 (b).

The comparison presented in this paper focuses on three key aspects. The first aspect is the fault current limiting capability, aiming to identify the stabilizer material that offers the most effective current-limiting performance. The second aspect is the temperature characteristics, as an excessive rise in temperature can lead to performance degradation and potential damage. Lastly, the third aspect examines the r-SFCL recovery time to select the stabilizer material that facilitates a shorter recovery time.

B. LITERATURE REVIEW

Superconductivity was discovered in 1911, when mercury was demonstrated to have zero electrical resistance at a critical temperature of 4.2 K [5]. Later, in 1986, High-temperature superconductivity (HTS) was discovered by Georg Bednorz and Alex Müller at IBM's Zurich Research Laboratory [6]. The discovery of HTS opened up multiple opportunities for power equipment. Key applications of HTS in power equipment include superconducting motors and generators, superconducting cables, SFCLs, and superconducting magnetic energy storage (SMES) systems.

Superconducting generators utilize superconducting materials to achieve high efficiency and power density. They proved its effectiveness in various applications [7], [8]. Among these applications, wind power had the highest

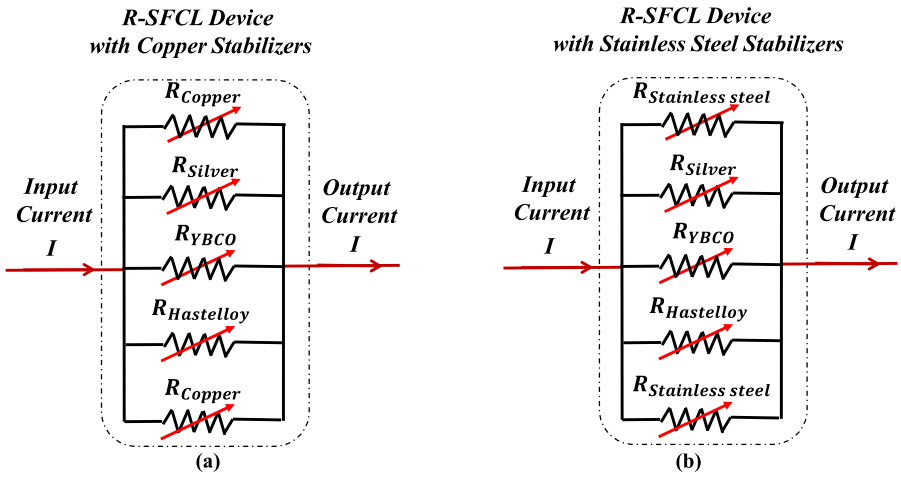

FIGURE 1. The r-SFCL equivalent circuits, (a) with copper stabilizers, (b) with stainless steel stabilizers.

technology readiness level of about 7 [9], followed by other applications, such as electric aircraft, wave energy, transportation, and so on. Superconducting motors, on the other hand, are suitable for transportation applications due to their smaller size, lighter weight, and higher efficiency compared to their conventional counterparts [10], [11]. Regarding superconducting cables, they are costly for AC power systems, but have good potential for DC ones [12]. As for SMES, they store electrical energy in a magnetic field, enabling them to quickly store and release large amounts of energy [13]. Thus, SMES systems can be used effectively in power smoothing [14], power quality improvement [15], and frequency control [16].

Fault current limiters (FCLs) are categorised into two main types: superconducting and non-superconducting. Non-superconducting FCLs have power losses during normal operation, which is undesirable for power system efficiency. With regards to SFCLs, they were used effectively in various applications covering both transmission and distribution systems. One such application is their utilization alongside distributed generating units to limit fault currents and maintain the original relay settings [17]. This is particularly important in power systems with a high penetration of RESs. Another application of SFCLs is providing virtual inertia by limiting the growth of current in case of disturbances [18]. SFCLs also play a crucial role in enhancing fault ride-through capabilities [19]. Furthermore, SFCLs could be integrated successfully with solid-state circuit breakers in DC systems to reduce the required current interruption rating of these circuit breakers [20].

There are two types of SFCLs: inductive SFCLs (i-SFCLs) and r-SFCLs. The r-SFCLs are less complex and lighter than other types of SFCLs [21]. To assess the performance of r-SFCLs, various modeling and experimental studies have been conducted. For example, in an electric aircraft environment, r-SFCLs have been modeled to support circuit breakers in scenarios with extremely high fault magnitudes [22]. The quench and recovery characteristics of r-SFCLs were investigated using both laboratory experiments as well as MATLAB®/Simulink simulations [23]. The recovery time was found to depend on the ratio of prospective current to critical current, and it can be immediate when this ratio falls below 5. In [24], the design of a single-phase r-SFCL was presented. This particular r-SFCL had a high rating of 220 kV and 1.5 kA, making it suitable for use in high-voltage applications. Within just 5 ms, the resistance of the r-SFCL could reach more than 50% of the required resistance.

The impact of stabilizer layer thickness on r-SFCLs has been investigated in previous studies [25], [26], revealing its influence on quench and recovery characteristics. The effects of shunt resistor value on r-SFCL performance have also been explored [27]. Increasing the shunt resistor results in faster recovery and reduced maximum temperature during faults, however the overall developed resistance is reduced.

The choice of stabilizer layer materials like copper and stainless steel in r-SFCLs significantly impacts their performance in several ways. Copper's conductivity is much better than that of stainless steel. The resistivity of copper at room temperature (20° C) is 1.7241×10^{-8} Ω.m [28]. On the other hand, the resistivity of stainless steel at room temperature is 77.1×10^{-8} Ω.m [29]. The other factor is the specific heat capacities of the two materials; the specific heat capacity is defined as the heat required to raise the temperature of the unit mass of a given substance by a given amount (degree). The specific heat capacities of copper and stainless steel at room temperature are 385 J/kg-K and 490 J/kg-K, respectively [29], [30]. More details regarding the two materials (copper and stainless steel) and their impact on r-SFCL performance will be discussed in section III.

C. CONTRIBUTIONS

First, a multilayer thermoelectric model was built for the r-SFCL in the MATLAB®/Simulink environment. Using this model, the stabilizer materials' impact on the r-SFCL's performance is investigated. Two superconducting tapes have

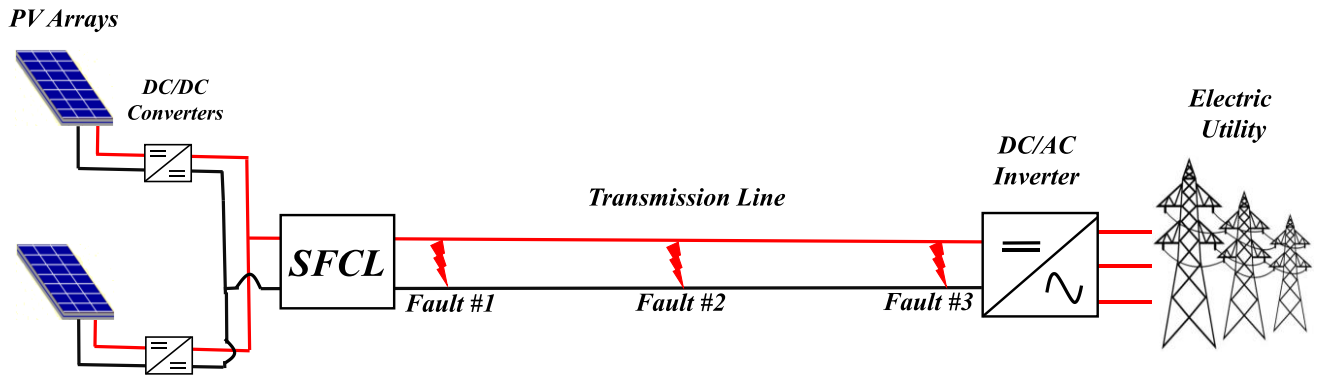

FIGURE 2. Overview of the system configuration with two PV arrays, DC transmission lines, and r-SFCL device.

been modeled in this study to illustrate the impact of the stabilizer materials on r-SFCL performance. The first tape consists of superconducting, silver, Hastelloy, and copper stabilizer layers, whereas the second tape consists of superconducting, silver, Hastelloy, and stainless steel stabilizer layers. The two r-SFCLs constructed by the two different superconducting tapes have been evaluated and compared in terms of fault current limiting capabilities, temperature, and recovery time in different fault scenarios. Three line-to-line faults have been applied to a solar farm's DC transmission line to investigate the r-SFCL's performance with the two different stabilizer materials. The first fault is located 5 km away from the solar farm, and the second and the third faults are located 15 and 25 km away from the solar farm, respectively, as shown in Fig. 2.

D. PAPER ORGANIZATION

After Section I, the paper is organized as follows: The system description is discussed in Section II. Section III describes the r-SFCL model with the two different stabilizer materials in detail, including electrical and thermal modeling. Section IV presents the simulation results obtained with different stabilizer materials. The results in Section IV are discussed in Section V. Finally, the conclusions of this study are presented in Section VI.

II. SYSTEM DESCRIPTION

The system under investigation in the current study is composed of a small-scale solar farm feeding an AC grid through DC transmission lines and a DC/AC inverter, as shown in Fig. 2. The solar farm is made up of two 250 kWp PV arrays with a total capacity of 500 kWp and an output voltage of 600 V. A boost DC/DC converter is utilized to link the output of PV arrays to the main DC bus, which operates at 3 kV_{DC}. Then, the DC bus is connected to the AC utility grid through the inverter. The r-SFCL device was installed on the DC transmission line at the solar farm side. The DC transmission line parameters, including the resistance and reactance, are considered crucial in studying the fault response of the system. These parameters can be determined in terms of the cable length (L), cable cross-sectional area (A), and material of the cable as follows:

$$R_{cu} = \rho_{cu}\frac{L}{A} \tag{1}$$

$$L_{wires} = \frac{\mu_0\mu_r}{\pi} cosh^{-1}\left(\frac{s}{d}\right).L \tag{2}$$

where ρ_{cu} is the copper resistivity and is equal to $1.7241 \times 10^{-8}\Omega$.m at 20 °C. The cable inductance can be determined by considering it as a pair of parallel conductors, where one conductor acts as the return path for the other one. The two conductors are spaced with a distance s, with each having a diameter of d. The permeability is expressed as the product of μ_0 and μ_r. The cable size of 300 mm^2 was chosen.

In this particular study, a line-to-line fault was considered and implemented at three different locations from the DC–DC converters, namely 5 km, 15 km, and 25 km. By considering these diverse fault locations, there will be variations in the prospective fault current and the current limitation capability of r-SFCLs. The system was simulated using the MATLAB®/Simulink software to examine how the performance of an r-SFCL is affected by various stabilizer materials across different fault locations. The specific details and characteristics of the r-SFCL device itself will be extensively discussed in Section III.

III. THERMOELECTRIC R-SFCL MODEL

When an electrical fault occurs, the fault current rapidly increases resulting in the temperature of an r-SFCL to rise above its critical temperature. This temperature rise causes the r-SFCL to transition to a resistive state, introducing a non-zero impedance to the circuit and effectively limiting the fault current. The entire transition process occurs within milliseconds, ensuring the continued safe operation of circuit breakers and switchgear [31]. Since thermoelectric transition is the main process responsible for an r-SFCL's performance, it is crucial to accurately model the thermoelectric behavior of the r-SFCL in this study.

SFCLs come in two types: r-SFCLs and i-SFCLs. The focus in this paper will be on the r-SFCL due to its advantages over the i-SFCL, which include being lighter, less

complicated, and less expensive [21], [32]. The utilized superconductor tapes in r-SFCLs govern its behavior. Two r-SFCLs devices are considered in this study to perform the comparison. The first r-SFCL device is made of Yttrium Barium Copper Oxide (YBCO) tapes and copper stabilizer layers, as shown in Fig. 1(a). The second r-SFCL device is made of YBCO tapes and stainless steel stabilizer layers, as illustrated in Fig. 1(b). Both r-SFCL devices are cooled to 77 K using liquid nitrogen (LN_2). The behavior of an r-SFCL is primarily influenced by the critical current density of the superconductor tape it employs (I_c) as well as its critical temperature (T_c). By maintaining the actual current (I) and temperature (T) below their critical values, the r-SFCL will be able to operate in the superconducting state. In this state, the full current flows through the YBCO layer of the superconductor tape, resulting in almost negligible resistivity.

When the current exceeds the critical current, the current is diverted to other layers of the tape due to the sharp increase in the YBCO layer's resistivity. Fig. 1(a) and (b) show the electrical representation of the r-SFCL devices with the two different stabilizer layers. The following equation is used to calculate the YBCO layer's resistivity (ρ_{YBCO}):

$$\rho_{YBCO} = \frac{E_c}{J_c(T)}\left(\frac{J}{J_c(T)}\right)^N J > J_C, T < T_c \tag{3}$$

where E_c is the standard electrical field, $J_c(T)$ is the critical current density, and N is the power-law exponent. The value of E_c is 1 μV/cm, while the experimentally estimated value of N falls within the range of 28 [25]. The critical current density is expressed in terms of the operating temperature (T_o), the current density at this temperature (J_{co}), and the actual temperature as follows:

$$J_c(T) = J_{co}\left(\frac{(T_c - T(t))^a}{(T_c - T_o)^a}\right) T_o < T < T_c \tag{4}$$

For liquid nitrogen cooling, the operating temperature is 77 K, while the critical temperature for YBCO is 93 K. The exponent α, known as the density exponent, is typically set to a value of 1.5 [33]. Equation (4) is applicable only for temperatures within the range of $T_o < T < T_c$. When the temperature surpasses T_c, the YBCO resistance increases, causing a significant portion of the current to be diverted to other layers. The resistivity of the remaining layers in the superconducting tape is dependent on temperature, with each material exhibiting a different temperature coefficient. Consequently, the resistivity of each layer is dynamically adjusted based on instantaneous temperature changes as follows:

$$\rho_{cu} = (0.0084 \times T - 0.4603) \times 10^{-8} \tag{5}$$

$$\rho_{ss} = (0.0844 * T + 51.551) \times 10^{-8} \tag{6}$$

$$\rho_{Ag} = 0.285 \times 10^{-8}[1 + \alpha(T - T_o)] \tag{7}$$

$$\rho_{Hast.} = (1.333 \times 10^{-10})T + 1.216 \times 10^{-6} \tag{8}$$

where ρ_{cu} and ρ_{ss} represent the resistivity of copper and stainless steel, respectively, depending on which is used as the stabilizer, ρ_{Ag} is silver's resistivity, and ρ_{Hast} is the Hastelloy's resistivity.

Based on the resistivities of all layers, the tape length (L), and the cross-sectional area of each layer (A_x), the total resistance of the r-SFCL can be determined using the following equations:

$$\frac{1}{R_{r-SFCL}} = \frac{1}{R_{YBCO}} + \frac{1}{R_{cu}} + \frac{1}{R_{Ag}} + \frac{1}{R_{Hastelloy}} \tag{9}$$

$$R_x = \rho_x \frac{L}{A_x} \tag{10}$$

where R_x and ρ_x represent the resistance and resistivity of each layer. The change in temperature impacts the resistivity of each layer. Thus, different amounts of current flow into different layers based on the updated temperature and Ohm's law. For this reason, it is crucial to accurately calculate the temperature of the r-SFCL.

The temperature of the superconductor tape is a function of the net tape power (Q_{sc}). This net tape power is obtained from the difference between heat generation within the tape due to electrical losses (P_{diss}) and the energy absorbed through the coolant ($P_{cooling}$), as detailed in the following equations:

$$T(t) = T_o + \frac{1}{C_p}\int_0^t Q_{sc}(t)\,dt \tag{11}$$

$$Q_{sc}(t) = P_{diss}(t) - P_{cooling}(t) \tag{12}$$

$$P_{diss}(t) = i(t)^2 R_{sc}(t) \tag{13}$$

$$P_{cooling}(t) = hA(T(t) - T_o) \tag{14}$$

where C_p is the cumulative heat capacity of the layers, h is the heat transfer coefficient between the tape and the LN_2 coolant, and A is the tape surface area in contact with the LN_2 coolant. The cumulative heat capacity of the layers is given as follows:

$$C_{P\_r-SFCL,Cu} = C_{P\_Hastelloy} + C_{P\_Cu} + C_{P\_Ag} \tag{15}$$

$$C_{P\_r-SFCL,ss} = C_{P\_Hastelloy} + C_{P\_SS} + C_{P\_Ag} \tag{16}$$

where (15) and (16) represent the cumulative heat capacity in case of the r-SFCL using the copper stabilizer and stainless steel stabilizer, respectively.

For the copper stabilizer-based r-SFCL, the heat capacity is determined by the dominant materials of this device, which are Hastelloy, copper, and silver, which can be calculated by (15). However, the dominant materials in the r-SFCL with stainless steel stabilizer are Hastelloy, stainless steel, and silver, which can be calculated by (16). The heat capacity of each material (C_{px}) can be determined by multiplying the specific heat capacity of this material (C_x) by its density (d_x) and volume (V_x), as described by the following equation:

$$C_{Px} = C_x \times d_x \times V_x \tag{17}$$

The specific heat capacity for stainless steel, copper, Hastelloy, and silver are sourced from [26], [30], [34], and [35]. The density for each material is shown in Table 1. The volume for each material can be determined using the tape specifications in Table 2.

TABLE 1. Densities of various materials used in studied superconducting tapes.

Material	Density (Kg/m^3)
Copper	8,940
Stainless Steel	7,980
Hastelloy	8,910
Silver	10,490

TABLE 2. The design parameters of the considered r-SFCLs.

Parameter	Value
Critical current	300 A
Conductor width	12 mm
YBCO layer thickness	1 µm
Hastelloy Substrate thickness	50 µm
Silver layer thickness	3.8 µm
Stabilizer thickness	20 µm × 2 layers
Total thickness	100 µm
Tape length	400 m
Number of tapes in parallel	1

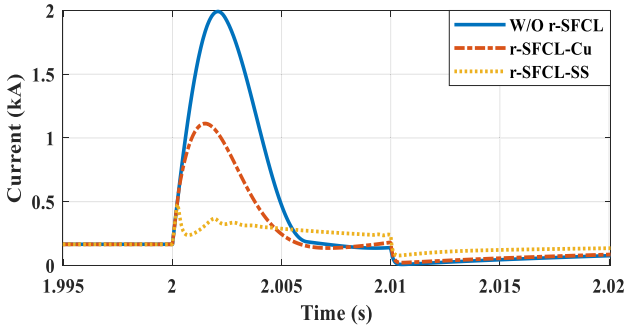

(a) The fault currents

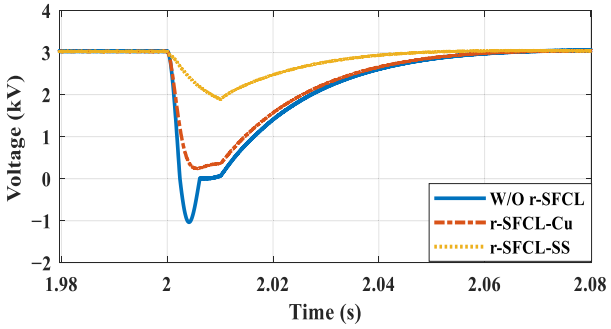

(b) The voltage drops

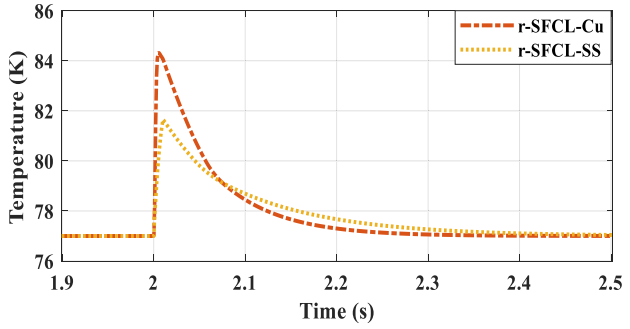

(c) The temperature profiles

FIGURE 3. Fault response at 5 km away from the solar farm.

IV. SIMULATION RESULTS

Fig. 2 illustrates the power system considered in this study. The MATLAB®/Simulink environment was used to model the system and evaluate the behavior of the r-SFCLs with the copper and stainless steel stabilizer layers when a fault occurs on a DC transmission line from a solar farm, as illustrated in Fig. 2. The fault type was a line-to-line fault and was located at different distances from the solar farm, corresponding to different line impedances. Based on (1) and (2), the line impedance was calculated to be 57 mΩ and 0.397 mH per km. Each DC/DC converter is equipped with a 0.5 mF capacitor. Three case studies are presented in this paper. Fault #1 is located 5 km away from the solar farm. Fault #2 is located 15 km away from the solar farm. Fault #3 is located 25 km away from the solar farm.

A. CASE STUDY 1 (COPPER VERSUS STAINLESS STEEL @ 5 km LENGTH)

In the first case study, where the line-to-the fault occurred 5 km away from the solar farm, the behavior of fault currents and other parameters were as visualized in Fig. 3. Fig. 3(a) depicts the fault currents in three scenarios. Firstly, the solid blue line represents the fault current without an r-SFCL, reaching a peak of 2 kA. This magnitude represents a multiple of 12 times the rated current. Secondly, the dash-dotted red line depicts the fault current when an r-SFCL with a copper stabilizer layer is employed. In this case, the fault current reaches a peak of 1.1 kA, equivalent to 6.63 times the rated current. Finally, the dotted yellow line represents the fault current with an r-SFCL featuring a stainless steel stabilizer layer. Here, the fault current reaches a peak of 480 A, which is 2.89 times the rated current. Fig. 3(b) illustrates the voltage drop for the DC transmission line in all three scenarios: without an r-SFCL, with the r-SFCL using the copper stabilizer, and with the r-SFCL using the stainless steel stabilizer. These scenarios are represented by solid blue, dash-dotted red, and dotted yellow lines, respectively. Fig. 3(c) depicts the temperature profiles of both r-SFCLs, with the copper

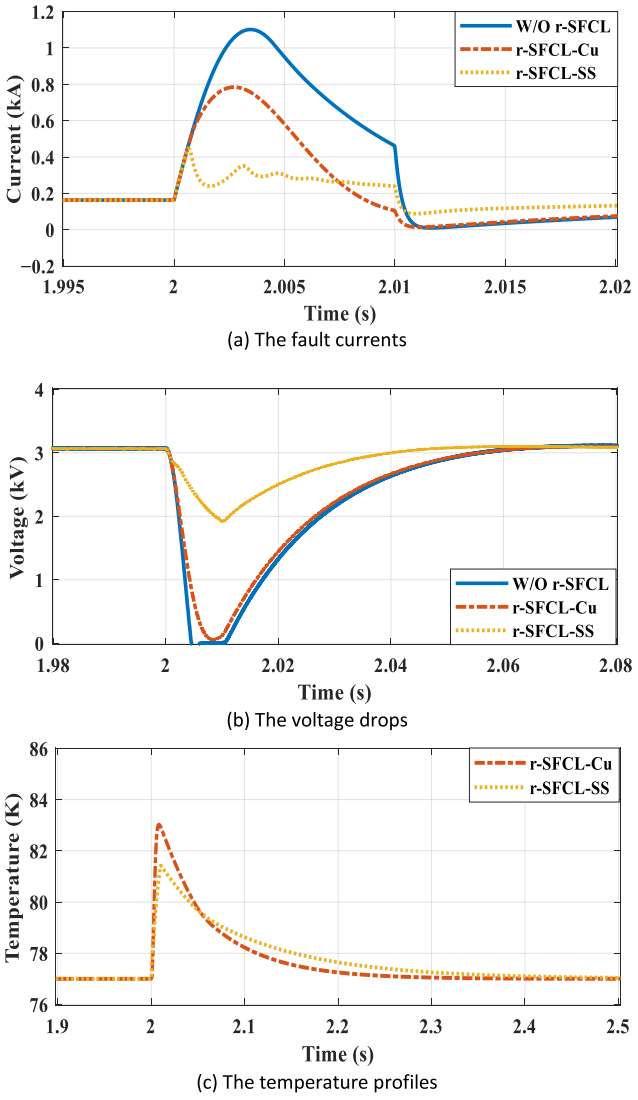

FIGURE 4. Fault response at 15 km away from the solar farm.

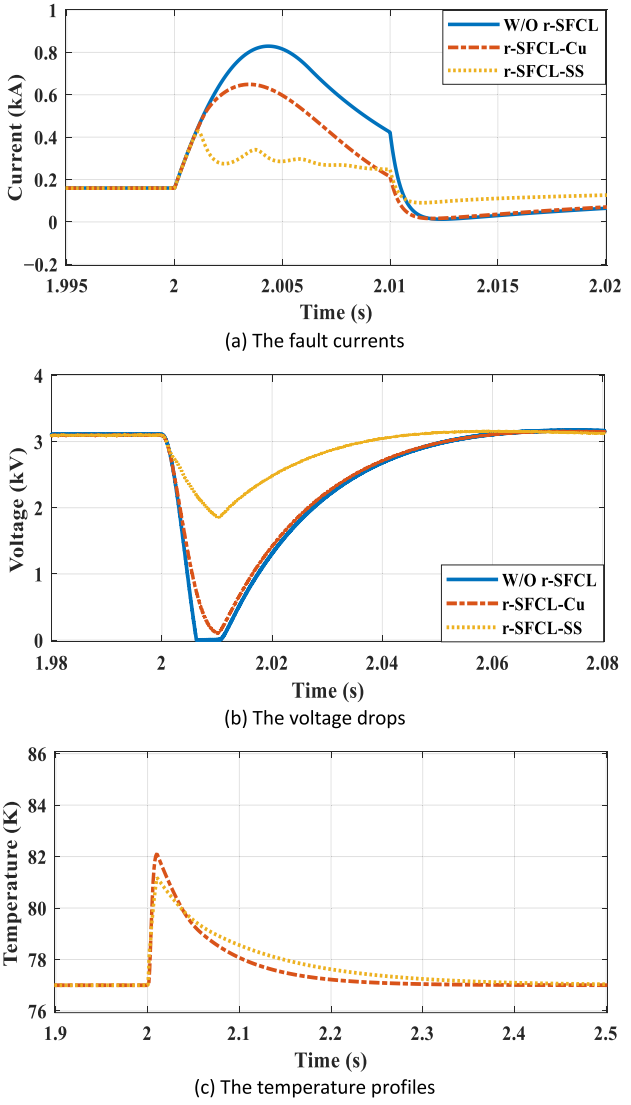

FIGURE 5. Fault Response at 15 km away from the solar farm.

stabilizer-based r-SFCL, denoted by the dash-dotted red line, reaching a temperature of 84.3 K, while the stainless steel stabilizer-based r-SFCL reached 81.5 K, as illustrated by the dotted yellow line.

B. CASE STUDY 2 (COPPER VERSUS STAINLESS STEEL @ 15 km LENGTH)

In the second case study, where the line-to-the fault occurred 15 km away from the solar farm, the fault currents and other parameters behaved as described and visualized in Fig. 4. Without an r-SFCL, the fault current reached 1.12 kA as represented by the solid blue line, 6.75 times the rated current. The dash-dotted red line represents the fault current when the r-SFCL incorporates the copper stabilizer layer, reaching a maximum of 790 A. This value is approximately 4.76 times the rated current. On the other hand, the dotted yellow line represents the fault current with the r-SFCL incorporating the stainless steel stabilizer layer, peaking at 450 A. This value corresponds to approximately 2.71 times the rated current. This demonstrates that the r-SFCL incorporating the stainless steel stabilizer offers superior fault current mitigation. Fig. 4(b) illustrates the voltage drop for the DC transmission line in those three scenarios: without an r-SFCL, with the r-SFCL using the copper stabilizer, and with the r-SFCL using the stainless steel stabilizer. These scenarios are represented by solid blue, dash-dotted red, and dotted yellow lines, respectively. Additionally, Fig. 4(c) depicts the temperature profile of the copper stabilizer-based r-SFCL, denoted by the dash-dotted red line, reaching a temperature of 83 K. In contrast, the r-SFCL with the stainless steel stabilizer reached 81.3 K, as shown by the dotted yellow line.

C. CASE STUDY 3 (COPPER VERSUS STAINLESS STEEL 25 km LENGTH)

In the third case study, with the line-to-the fault occurring 25 km away from the solar farm, the fault currents were as

depicted in Fig. 5(a). Without an r-SFCL, the fault current peaked at 820 A, exceeding the rated current by a factor of 4.94. When the r-SFCL with the copper stabilizer layer was employed, the fault current was limited to 650 A (3.91 times the rated current), while the r-SFCL with the stainless steel stabilizer limited the fault current to 415 A (2.5 times the rated current). Fig. 5(b) illustrates the corresponding voltage drop for the DC transmission line during those three scenarios, while Fig. 5(c) depicts the temperature profiles of the r-SFCLs. The r-SFCL temperature reached 82 K when using the copper stabilizer, whereas the temperature reached 81.1 K when using the stainless steel stabilizer.

V. DISCUSSIONS

The impact of the fault's location on the fault's behavior is discussed in this section. This section illustrates the effect of the stabilizer material on the r-SFCL's fault current limiting capability. The stabilizer materials' impact on the r-SFCL is explained. Finally, the recovery time of the r-SFCLs with the two stabilizer layers is discussed.

The location of the fault on the transmission line greatly impacts the fault current magnitude. When the fault occurred 5 km away from the solar farm, it resulted in a prospective current of 2 kA if no r-SFCL was used, whereas when the fault occurred 15 km away from the solar farm, the fault current decreased to 1.12 kA without an r-SFCL, a reduction of 44% compared to the first case study. In the third case study, when the fault occurred 25 km away from the solar farm, the fault current magnitude dropped to 820 A, a reduction of 59% compared to the first case study. The magnitude of the fault currents when no r-SFCL is used, as well as the ratio when compared to the rated current, in the three case studies are presented in Table 3 alongside the distance from the solar farm to the fault location in each case.

TABLE 3. The severity of the fault with respect to the fault distance from the power source (Solar Farm).

Case Study #	Without r-SFCL (A)	I fault/ I rated
1 (5 km)	2,000	12
2 (15 km)	1,120	6.75
3 (25 km)	820	4.94

Table 3 clearly shows that fault current magnitudes can be hazardously high when the fault occurs close to the power source, reaching 12 times the rated current when the fault was 5 km away from the solar farm in this case. This clearly shows the increased need for r-SFCL devices to immediately react to such faults, reducing the fault current magnitude, and allowing the DC CB to operate safely. However, the importance of using r-SFCL devices drops the farther the fault location is from the power source. When the fault occurred only 20 km away from the first case study, the fault current dropped by 59% compared to the first case study.

The material of the stabilizer layer greatly affects the r-SFCL's fault current limiting capability. In the first case study, when the fault occurred 5 km away from the solar farm, the fault current magnitude with the copper stabilizer-based r-SFCL was 1.1 kA, whereas the fault magnitude was 480 A with the r-SFCL using the stainless steel stabilizer, a reduction of 56.4% compared to the fault current magnitude that the copper stabilizer-based r-SFCL achieved. This comes from the fact that the resistivity of stainless steel (77.1×10^{-8} Ω.m @ 20°C) is 44.7 times the resistivity of copper (1.7241×10^{-8} Ω.m @ 20°C), and based on Ohm's law, when the value of the resistance increase, the current passing through that resistance will decrease at a fixed voltage. Thus, the higher resistance for the stainless steel stabilizer and a fixed voltage in both cases will result in a lower current in the r-SFCL incorporating the stainless steel stabilizer. Similarly in the third case study, when the fault occurred 20 km away from the first case's fault location, the fault current magnitude with r-SFCL with copper stabilizer was 650 A, whereas it was 415 A with the r-SFCL incorporating the stainless steel stabilizer, representing a reduction of 36.15% compared to the fault current magnitude with the copper stabilizer-based r-SFCL.

Table 4 shows the stabilizer layer impact on the fault current magnitude. Table 4 clearly shows that while fault current magnitudes were reduced by using either r-SFCL, the reductions offered by the r-SFCL with the stainless steel stabilizer were higher. The fault current magnitudes achieved by the r-SFCL with the stainless steel stabilizer were lower by 56.4%, 43.04%, and 36.15% compared to the fault currents observed when using the copper stabilizer-based r-SFCL in case studies 1, 2, and 3, respectively. When the fault location is farther from the power source (solar farm), the fault current magnitude decreases, and as a result, the difference between the two r-SFCLs fault current limiting capabilities is reduced. As shown in Table 4, the differences in the fault current limiting capability of the two r-SFCLs increase when the fault magnitude rises.

TABLE 4. Comparing fault current magnitudes in the r-SFCL with different materials as a stabilizer.

Case Study #	Without r-SFCL (A)	R-SFCL Cu Stabilizer (A)	R-SFCL SS Stabilizer (A)	R-SFCL Cu Vs. R-SFCL SS (%)
1 (5 km)	2,000	1,100	480	56.4
2 (15 km)	1,120	790	450	43.04
3 (25 km)	820	650	415	36.15

It is noted from Table 4 that the stainless steel stabilizer-based r-SFCL is less sensitive to the fault location than the copper stabilizer-based r-SFCL. With the copper

stabilizer-based r-SFCL, the fault magnitude was 1.1 kA at the 5 km fault location, whereas the fault magnitude was 650 A at the 25 km with a difference of 450 A, a change of 40.9% compared to the fault current magnitude at 5 km. However, with the stainless steel stabilizer-based r-SFCL the fault magnitude was 480 A at the 5 km fault location, whereas the fault magnitude was 415 A at the 25 km with a difference of only 65 A, a change of 13.54% compared to the fault current magnitude at 5 km.

It is always desirable to have a low magnitude fault current, as with the stainless steel stabilizer-based r-SFCL, to support the protection system, allowing CBs to operate safely. However, a very low sensitivity to the fault location can pose another protection challenge to the protection scheme of an electrical network, which is the coordination of the overcurrent relays. The impact of the r-SFCL with different stabilizer materials on the coordination of the overcurrent relays will be discussed in detail in future work.

The material of the stabilizer layer affects the fault current limiting capability of the r-SFCL and impacts the r-SFCL temperature. In the first case study, when the fault occurred 5 km away from the solar farm, the r-SFCL temperature was 84.3 K when utilizing the copper stabilizer layer, while it reached 81.5 K when employing the stainless steel stabilizer. The temperature of the stainless steel-based r-SFCL was lower than that of the copper stabilizer-based r-SFCL in all case studies for two reasons. The first reason is that the heat generated in the r-SFCL. As per (13), as the current increases, a corresponding increase occurs in heat generated within the r-SFCL. Given that the resistivity of stainless steel is higher than that of copper, a higher current passes through the r-SFCL with the copper stabilizer layer, resulting in greater heat generation compared to the r-SFCL with the stainless steel stabilizer layer. The second reason is that the specific heat capacity of stainless steel is higher than that of copper. Based on (11), when the heat capacity is higher, the change in the temperature is lower, leading to more rapid temperature changes in the r-SFCL with the copper stabilizer. Table 5 shows the temperatures of the r-SFCLs with both stabilizer layers across all case studies.

TABLE 5. Temperatures of the r-SFCLs with both stabilizer layers for all case studies.

CASE STUDY #	R-SFCL Cu Temp. (K)	R-SFCL SS Temp. (K)
1 (5 km)	84.3	81.5
2 (15 km)	83	81.3
3 (25 km)	82	81.1

Despite the higher temperatures exhibited by the r-SFCL with the copper stabilizer in all three case studies, the recovery times for the r-SFCL with the stainless steel were actually longer than the recovery times of the r-SFCL with copper in the three case studies because of the specific heat of the two materials. The specific heat capacities of copper and stainless steel at room temperature are 385 J/kg-K and 490 J/kg-K, respectively, which means that more energy is needed to raise or reduce the temperature of a given mass of stainless steel compared to the same mass of copper.

VI. CONCLUSION

This study investigated the behavior of an r-SFCL in a DC transmission line fed from a solar farm when using different materials for the stabilizer layers. The considered fault type was a line-to-line fault, with three different fault locations used in the analysis. The fault location had a strong impact on the fault current magnitude. When the fault occurred 5 km from the solar farm, the current magnitude was 2 kA, whereas the current magnitude was 820 A when the fault occurred 25 km from the solar farm. The difference between the three cases was primarily due to the change in line impedance as the fault location varied. These findings highlight the high importance of r-SFCL devices, particularly for faults that occur near power sources such as solar farms.

The material of the stabilizer layer affected greatly the r-SFCL performance. When the fault occurred 5 km from the solar farm, the r-SFCL with the stainless steel stabilizer limited the fault current magnitude to 480 A, whereas the copper stabilizer-based r-SFCL allowed a fault current magnitude of 1.1 kA. This difference can be attributed to the high resistivity of stainless steel, which is about 44.7 times that of copper. With the copper stabilizer, the r-SFCL's temperature reached 84.3 K, while it reached 81.5 K when using the stainless steel stabilizer. The lower temperature observed in the r-SFCL with stainless steel can be attributed to the lower current flow in the stabilizer layer compared to the copper stabilizer. Furthermore, stainless steel has a lower specific heat capacity compared to copper, which means it requires less energy to raise its temperature.

On the other hand, the sensitivity of the fault location is higher with the copper stabilizer-based r-SFCL than with the stainless steel stabilizer-based r-SFCL. With the copper stabilizer-based r-SFCL, the difference between the fault magnitude at the 5 km fault location and the 25 km fault location was 450 A, a change of 40.9% compared to the fault current magnitude at the 5 km. However, with the stainless steel stabilizer-based r-SFCL, the difference between the fault magnitude at the 5 km fault location and the 25 km fault location was 65 A, a change of 13.54% compared to the fault current magnitude at the 5 km. The variation of the fault current magnitudes with respect to the fault location is strongly required in the coordination of overcurrent relays. Low sensitivity to the fault location, as with the stainless steel stabilizer-based r-SFCL, poses another protection challenge for the electrical network, which is the overcurrent relays coordination.

This article highlights the importance of r-SFCL devices for DC systems, particularly when faults occur near power sources. These devices play a crucial role in reducing the

magnitude of fault currents, thereby reducing the current interruption rating of DC CBs. Stainless steel performs better than copper as a stabilizer layer in r-SFCL devices in terms of fault current limiting capability, voltage behaviors, and operating temperature, whereas copper performs better than stainless steel as a stabilizer layer in r-SFCL devices in terms of sensitivity to the fault location. The excellent performance of the r-SFCL with stainless steel stabilizers in terms of its fault current limiting capability makes it a promising device to support the protection scheme in DC power systems, electric aircraft, and electric ships where fault current magnitudes are expected to be high. In future work, the sensitivity to the fault location and the challenge of the overcurrent relays coordination in electrical networks with r-SFCL devices with different stabilizer materials will be discussed in detail.

REFERENCES

[1] Z. Ali, Y. Terriche, L. Q. N. Hoang, S. Z. Abbas, M. A. Hassan, M. Sadiq, C.-L. Su, and J. M. Guerrero, "Fault management in DC microgrids: A review of challenges, countermeasures, and future research trends," *IEEE Access*, vol. 9, pp. 128032–128054, 2021, doi: 10.1109/ACCESS.2021.3112383.

[2] N. Bayati, H. R. Baghaee, M. Savaghebi, A. Hajizadeh, M. N. Soltani, and Z. Lin, "DC fault current analyzing, limiting, and clearing in DC microgrid clusters," *Energies*, vol. 14, no. 19, p. 6337, Oct. 2021, doi: 10.3390/en14196337.

[3] Superpower Inc. *2G HTS Wire Specification*. Accessed: Apr. 3, 2024. [Online]. Available: https://www.superpower-Inc.com/specification.aspx

[4] American Superconductor. (8602). *Amperium® Stainless Steel Laminated Wire Type 8602*. [Online]. Available: https://www.amsc.com/wp-content/uploads/SSAMP8602_DS_A4_0414_WEB.pdf

[5] D. van Delft and P. Kes, "The discovery of superconductivity," *Phys. Today*, vol. 63, no. 9, pp. 38–43, Sep. 2010, doi: 10.1063/1.3490499.

[6] M. Kenward, "Superconductors get ready to transform industry," *Phys. World*, vol. 9, no. 6, pp. 29–32, Jun. 1996, doi: 10.1088/2058-7058/9/6/26.

[7] F. Weng, M. Zhang, A. Elwakeel, T. Lan, N. McNeill, and W. Yuan, "Transient test and AC loss study of a cryogenic propulsion unit for all electric aircraft," *IEEE Access*, vol. 9, pp. 59628–59636, 2021, doi: 10.1109/ACCESS.2021.3073071.

[8] X. Song, C. Bührer, A. Mølgaard, R. S. Andersen, P. Brutsaert, M. Bauer, J. Hansen, A. V. Rebsdorf, J. Kellers, T. Winkler, A. Bergen, M. Dhalle, S. Wessel, M. T. Brake, J. Wiezoreck, H. Kyling, H. Boy, and E. Seitz, "Commissioning of the World's first full-scale MW-class superconducting generator on a direct drive wind turbine," *IEEE Trans. Energy Convers.*, vol. 35, no. 3, pp. 1697–1704, Sep. 2020, doi: 10.1109/TEC.2020.2982897.

[9] B. M. O. Santos, F. J. M. Dias, F. Trillaud, G. G. Sotelo, and R. de Andrade Junior, "A review of technology readiness levels for superconducting electric machinery," *Energies*, vol. 16, no. 16, p. 5955, Aug. 2023, doi: 10.3390/en16165955.

[10] M. Yazdani-Asrami, M. Zhang, and W. Yuan, "Challenges for developing high temperature superconducting ring magnets for rotating electric machine applications in future electric aircrafts," *J. Magn. Magn. Mater.*, vol. 522, Mar. 2021, Art. no. 167543, doi: 10.1016/j.jmmm.2020.167543.

[11] D. Torrey, M. Parizh, J. Bray, W. Stautner, N. Tapadia, M. Xu, A. Wu, and J. Zierer, "Superconducting synchronous motors for electric ship propulsion," *IEEE Trans. Appl. Supercond.*, vol. 30, no. 4, pp. 1–8, Jun. 2020, doi: 10.1109/TASC.2020.2980844.

[12] M. Yazdani-Asrami, S. Seyyedbarzegar, A. Sadeghi, W. T. B. de Sousa, and D. Kottonau, "High temperature superconducting cables and their performance against short circuit faults: Current development, challenges, solutions, and future trends," *Superconductor Sci. Technol.*, vol. 35, no. 8, Aug. 2022, Art. no. 083002, doi: 10.1088/1361-6668/ac7ae2.

[13] H. Alafnan, X. Pei, M. Khedr, I. Alsaleh, A. Albaker, M. Alturki, and D.-E.-A. Mansour, "The possibility of using superconducting magnetic energy storage/battery hybrid energy storage systems instead of generators as backup power sources for electric aircraft," *Sustainability*, vol. 15, no. 3, p. 1806, Jan. 2023, doi: 10.3390/su15031806.

[14] M. E. Elshiekh, D. A. Mansour, M. Zhang, W. Yuan, H. Wang, and M. Xie, "New technique for using SMES to limit fault currents in wind farm power systems," *IEEE Trans. Appl. Supercond.*, vol. 28, no. 4, pp. 1–5, Jun. 2018, doi: 10.1109/TASC.2018.2810512.

[15] D. Çelik and H. Ahmed, "Enhanced control of superconducting magnetic energy storage integrated UPQC for power quality improvement in EV charging station," *J. Energy Storage*, vol. 62, Jun. 2023, Art. no. 106843, doi: 10.1016/j.est.2023.106843.

[16] D. K. Mishra, D. Złotecka, and L. Li, "Significance of SMES devices for power system frequency regulation scheme considering distributed energy resources in a deregulated environment," *Energies*, vol. 15, no. 5, p. 1766, Feb. 2022, doi: 10.3390/en15051766.

[17] Y. Kim, H.-C. Jo, and S.-K. Joo, "Analysis of impacts of superconducting fault current limiter (SFCL) placement on distributed generation (DG) expansion," *IEEE Trans. Appl. Supercond.*, vol. 26, no. 4, pp. 1–5, Jun. 2016, doi: 10.1109/TASC.2016.2550598.

[18] D. M. Yehia and I. B. M. Taha, "Application of superconducting fault current limiter as a virtual inertia for DC distribution systems," *IEEE Access*, vol. 9, pp. 135384–135391, 2021, doi: 10.1109/ACCESS.2021.3115989.

[19] L. Chen, M. Ding, H. Chen, X. Wang, X. Deng, G. Li, Y. Li, F. Xia, L. Wang, and H. He, "Study on resistive SFCL for fault ride-through fulfillment of power electronic transformer interconnecting MV and LV power systems," *IEEE Trans. Appl. Supercond.*, vol. 31, no. 8, pp. 1–6, Nov. 2021, doi: 10.1109/TASC.2021.3101746.

[20] J. Xi, X. Pei, W. Song, L. Niu, Y. Liu, and X. Zeng, "Integration of superconducting fault current limiter with solid-state DC circuit breaker," *Int. J. Electr. Power Energy Syst.*, vol. 145, Feb. 2023, Art. no. 108630, doi: 10.1016/j.ijepes.2022.108630.

[21] W. T. B. de Sousa, R. Dias, F. A. da Silva, A. Polasek, and R. de Andrade, "Comparison between the fault current limiting performance of bi-2212 bifilar components and 2G YBCO coils," *IEEE Trans. Appl. Supercond.*, vol. 23, no. 3, pp. 2–6, Jun. 2013, doi: 10.1109/TASC.2013.2238275.

[22] H. Alafnan, X. Zeng, X. Pei, M. Khedr, M. Zhang, and W. Yuan, "Analysing faults and SFCL response in electric aircraft," *J. Phys., Conf. Ser.*, vol. 1559, no. 1, Jun. 2020, Art. no. 012103, doi: 10.1088/1742-6596/1559/1/012103.

[23] W. Song, X. Pei, H. Alafnan, J. Xi, X. Zeng, M. Yazdani-Asrami, B. Xiang, and Z. Liu, "Experimental and simulation study of resistive helical HTS fault current limiters: Quench and recovery characteristics," *IEEE Trans. Appl. Supercond.*, vol. 31, no. 5, pp. 1–6, Aug. 2021, doi: 10.1109/TASC.2021.3061958.

[24] S. Dai, T. Ma, C. Xue, L. Zhao, Y. Huang, L. Hu, B. Wang, T. Zhang, X. Xu, L. Cai, and H. Chen, "Development and test of a 220 kV/1.5 kA resistive type superconducting fault current limiter," *Phys. C, Supercond. Appl.*, vol. 565, Oct. 2019, Art. no. 1253501, doi: 10.1016/j.physc.2019.06.004.

[25] B. Xiang, M. Junaid, L. Gao, Z. Liu, Y. Geng, J. Wang, and S. Yanabu, "Influencing factors on quench and recovery of YBCO tapes for DC superconducting fault current limiter," *IEEE Trans. Appl. Supercond.*, vol. 29, no. 2, pp. 1–6, Mar. 2019, doi: 10.1109/TASC.2018.2887336.

[26] H. Alafnan, X. Pei, D.-E.-A. Mansour, M. Khedr, W. Song, I. Alsaleh, A. Albaker, M. Alturki, and X. Zeng, "Impact of copper stabilizer thickness on SFCL performance with PV-based DC systems using a multilayer thermoelectric model," *Sustainability*, vol. 15, no. 9, p. 7372, Apr. 2023, doi: 10.3390/su15097372.

[27] H. Alafnan, D.-E.-A. Mansour, X. Pei, M. Khedr, M. Alturki, A. Albaker, I. Alsaleh, and X. Zeng, "Effect of shunt resistor value on the performance of resistive superconducting fault current limiters," *Appl. Sci.*, vol. 13, no. 20, p. 11339, Oct. 2023, doi: 10.3390/app132011339.

[28] R. A. Matula, "Electrical resistivity of copper, gold, palladium, and silver," *J. Phys. Chem. Reference Data*, vol. 8, no. 4, pp. 1147–1298, Oct. 1979.

[29] C. Y. Ho and T. K. Chu, "Electrical resistivity and thermal conductivity of nine selected AISI stainless steels," Thermophys. Electron. Prop. Inf. Anal. Cent., Lafayette, IN, USA, Tech. Rep. CINDAS-45, 1977.

[30] B. Banerjee, "An evaluation of plastic flow stress models for the simulation of high-temperature and high-strain-rate deformation of metals," 2005, .

[31] X. Pei, A. C. Smith, and M. Barnes, "Superconducting fault current limiters for HVDC systems," *Energy Proc.*, vol. 80, pp. 47–55, Jan. 2015.

[32] S. Naderi, P. Davari, D. Zhou, M. Negnevitsky, and F. Blaabjerg, "A review on fault current limiting devices to enhance the fault ride-through capability of the doubly-fed induction generator based wind turbine," *Appl. Sci.*, vol. 8, no. 11, p. 2059, Oct. 2018, doi: 10.3390/app8112059.

[33] M. Elshiekh, M. Zhang, H. Ravindra, X. Chen, S. Venuturumilli, X. Huang, K. Schoder, M. Steurer, and W. Yuan, "Effectiveness of superconducting fault current limiting transformers in power systems," *IEEE Trans. Appl. Supercond.*, vol. 28, no. 3, pp. 1–7, Apr. 2018, doi: 10.1109/TASC.2018.2805693.

[34] J. Lu, E. S. Choi, and H. D. Zhou, "Physical properties of Hastelloy® C-276™ at cryogenic temperatures," *J. Appl. Phys.*, vol. 103, no. 6, pp. 1–6, Mar. 2008, doi: 10.1063/1.2899058.

[35] D. R. Smith and F. R. Fickett, "Low-temperature properties of silver," *J. Res. Nat. Inst. Standards Technol.*, vol. 100, no. 2, p. 119, Mar. 1995, doi: 10.6028/jres.100.012.

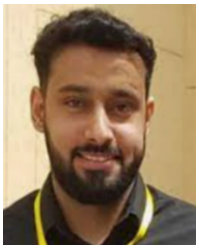

HAMOUD ALAFNAN received the B.S. degree in electrical engineering from the University of Ha'il, Saudi Arabia, in June 2011, the M.S. degree in electrical engineering from the University of New Haven, USA, in May 2016, with an emphasis in smart grids, and the Ph.D. degree in electronic and electrical engineering from the University of Bath, U.K., in February 2021, with an emphasis on power system protection. He is currently an Assistant Professor with the Electrical Engineering Department, University of Ha'il, where he has been, since February 2021. His research interests include smart grids, power protection systems, superconductivity, energy storage systems, and fault current limiters.

DOAA M. YEHIA received the B.Sc. and M.Sc. degrees in electrical engineering from Tanta University, Egypt, in 2002 and 2006, respectively, and the Ph.D. degree in electrical engineering from Nagoya University, Nagoya, Japan, in 2011. Since 2003, she has been with the Department of Electrical Power and Machines Engineering, Faculty of Engineering, Tanta University, as an Instructor, an Assistant Lecturer, and a Lecturer, where she is currently an Assistant Professor. Her research interests include dc distribution systems, renewable energy, energy storage systems, and smart grids.

ABDULLAH ALBAKER received the M.S. and Ph.D. degrees in electrical engineering from the University of Denver, Denver, CO, USA, in 2014 and 2018, respectively, specializing in electric power engineering. He is currently an Associate Professor of electrical engineering with the University of Ha'il, Hail, Saudi Arabia. His research interests include microgrid planning and operation, renewable energy and distributed generation, power systems reliability, economics and optimization, machine learning, and smart electricity grids.

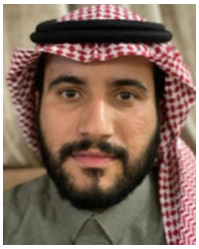

AYOOB ALATEEQ received the B.S. degree in electrical engineering from the University of Ha'il, Hail, Saudi Arabia, in 2009, and the M.S. and Ph.D. degrees from the University of Denver, in 2013 and 2018, respectively. Since 2019, he has been an Assistant Professor with the Department of Electrical Engineering, University of Ha'il. His current research interest includes optimization in dc conversation.